AIAA AVIATION Forum
13-17 June 2016, Washington, D.C.
34th AIAA Applied Aerodynamics Conference

10.2514/6.2016-3865

Aerodynamic Shape Optimization by Variable-fidelity Models and Gradient-Enhanced Manifold Mapping

Leifur Leifsson[1]
Iowa State University, Ames, Iowa, 50011

Yonatan Tesfahunegn[2] and Slawomir Koziel[3]
Engineering Optimization & Modeling Center, Reykjavik University, Reykjavik, Iceland

This paper describes an extension to the manifold mapping (MM) optimization algorithm for aerodynamic shape design to include gradients through the calculation of adjoint sensitivities. The gradient information is used to enhance the MM surrogate, and to speed up the optimization process. Moreover, the addition of gradients based on adjoint sensitivity allows for handling of large-dimensional design spaces. The gradient-enhanced manifold mapping (GMM) algorithm replaces the direct optimization of a computationally expensive model by an iterative updating and re-optimization of a fast physics-based replacement surrogate model. During the optimization process the GMM surrogate is constructed using a low-fidelity model which is corrected using high-fidelity data (evaluated once per design iteration). The performance of the method is demonstrated on a benchmark case involving drag minimization in two-dimensional transonic inviscid flow. For the demonstration case, the results show that GMM obtains comparable designs as MM with 70% less computing time.

I. Introduction

The development of efficient optimization algorithms is key for rapid design of simulation-based engineering systems.[1,2] Modern engineering design often requires CPU-intensive high-fidelity simulations to capture the nonlinear physics and multidisciplinary couplings. Although high-performance computing is routinely used throughout the analysis and optimization process the high computational cost of the simulations and the multi-dimensional design space creates a design problem which can be impractical to solve with conventional optimization techniques[3-9].

In surrogate-based optimization[10-13] (SBO), the direct optimization of the high-fidelity model is replaced by an iterative correction-prediction process where a surrogate model is constructed and then utilized to find an approximate location of the high-fidelity model optimal design. There are many SBO approaches available and they differ mainly in how the surrogate model is constructed and updated. Data-driven surrogates are constructed by approximating sampled high-fidelity model data using techniques such as polynomial approximation, radial basis functions, kriging, neural networks, or support vector regression (see, for example, Queipo *et al.*[10], and Forrester and Keane[11]). Physics-based surrogates (or multi-fidelity surrogates) are constructed using physics-based low-fidelity models[12-14] which are corrected or enhanced to become a reliable representation of the high-fidelity model using methods such as multiplicative or additive corrections,[12] space mapping[15,16] (SM), adaptive response correction[17] (ARC), adaptive response prediction[18] (ARP), or shape-preserving response prediction[19] (SPRP).

Data-driven surrogates can be the basis of efficient global optimization techniques,[11] but to ensure adequate accuracy, these surrogates require a large number of data samples. Unfortunately, the number of samples grows quickly with the problem dimensionality. The physics-based surrogate models are not as versatile as the data-driven ones. Nevertheless, they have the potential to offer significantly better efficiency in terms of the computational cost.[12-14] In fact, many physics-based SBO algorithms need only a single high-fidelity model evaluation per design iteration.[12] In this work, we focus on optimization using physics-based surrogate models.

Several physics-based SBO algorithms have been developed over the years. These algorithms can be broadly categorized into parametric (where the correction or enhancement functions are given explicitly with the parameters

[1] Assistant Professor, Department of Aerospace Engineering, AIAA Senior Member.
[2] Post-doctoral Fellow, School of Science and Engineering, AIAA Member.
[3] Professor, School of Science and Engineering, AIAA Senior Member.

usually obtained by explicit calculations or by solving auxiliary linear regression problems) and non-parametric. The parametric algorithms include approximation and model management optimization[13] (AMMO) involving first- and higher-order correction terms, multi-point correction techniques,[15,16] several variations of output space mapping[15] (SM), as well as manifold mapping[20,21] (MM). ARC[17], ARP[18], and SPRP[19] are all non-parametric algorithms.

Recently, MM was applied to aerodynamic shape optimization in its basic version[22]. In this work, we extend the basic MM algorithm for aerodynamic shape optimization[22] to include adjoint sensitivity information[23]. This extension improves the MM surrogate model as well as accelerates the MM-based SBO process. Moreover, the adjoint-enhanced MM algorithm is capable of handling large-dimensional design spaces (over 40 design variables). Due to the computational expense, the basic version is limited to small-dimensional (less than 10 design variables) to medium-dimensional (between 10 and 40 design variables) design spaces.[22]

The paper is organized as follows. We begin by giving the details of the proposed optimization algorithm. The proposed approach is applied to a benchmark aerodynamic design problem involving inviscid transonic airfoil flow. The paper ends with conclusions.

II. Optimization Methodology

This section describes the proposed aerodynamic shape optimization (ASO) algorithm. In particular, the details of the problem formulation, a generic variable-fidelity optimization algorithm, and manifold mapping with and without gradient information are given.

A. Problem Formulation

ASO problems can be formulated as constrained nonlinear minimization problems in the following way:

$$\mathbf{x}^* = \arg\min_{\mathbf{x}} H(\mathbf{f}(\mathbf{x})) \text{ s.t. } \mathbf{g}(\mathbf{x}) \le 0, \mathbf{h}(\mathbf{x}) = 0, \ \mathbf{l} \le \mathbf{x} \le \mathbf{u}, \tag{1}$$

where $\mathbf{x}$ is the design variable vector of size $p \times 1$, $\mathbf{x}^*$ is the optimized design, H is a scalar valued objective function, $\mathbf{f}(\mathbf{x})$ is a vector of size $q \times 1$ with the figures of merit, $\mathbf{g}(\mathbf{x})$ is a vector of size $M \times 1$ with the inequality constraints, $\mathbf{h}(\mathbf{x})$ is a vector of size $N \times 1$ with the equality constraints, and $\mathbf{l}$ and $\mathbf{u}$ are the design variable lower and upper bounds, respectively, both vectors of the same size as $\mathbf{x}$. Here, the vectors $\mathbf{f}(\mathbf{x})$, $\mathbf{g}(\mathbf{x})$, and $\mathbf{h}(\mathbf{x})$ are all obtained or derived from aerodynamic models requiring computationally expensive simulations of partial differential equations (PDEs).

In this work, the high-fidelity aerodynamics model calculates the figures of merit $\mathbf{f}(\mathbf{x}) = [C_{l.f}(\mathbf{x})\ C_{d.f}(\mathbf{x})\ A(\mathbf{x})]^T$, where $C_{l.f}(\mathbf{x})$ is the nondimensional lift coefficient, $C_{d.f}(\mathbf{x})$ is the nondimensional drag coefficient, and $A(\mathbf{x})$ the airfoil cross-sectional area. The subscript f denotes the high-fidelity model. In the case of a lift-constrained drag minimization problem, the objective function in (1) is set as $H(\mathbf{f}(\mathbf{x})) = C_{d.f}(\mathbf{x})$, and the inequality constraints are set as $g_1(\mathbf{x}) = C_{m.min} - C_{m.f}(\mathbf{x}) \le 0$, and $g_2(\mathbf{x}) = A_{min} - A(\mathbf{x}) \le 0$, where $C_{m.min}$ is a minimum allowable pitching moment coefficient, $C_{m.f}(\mathbf{x})$ is the pitching moment of the current design $\mathbf{x}$, A_{min} is a minimum cross-sectional area, and $A(\mathbf{x})$ the cross-sectional area of the design $\mathbf{x}$. The equality constraint is $h_1(\mathbf{x}) = C_{l.t} - C_{l.f}(\mathbf{x}) = 0$, where $C_{l.t}$ is the target lift coefficient, and $C_{l.f}(\mathbf{x})$ is the lift coefficient of the current design. In this work, the angle of attackis used as a dummy variable to find the target lift coefficient value. All the constraints are handled directly in the optimization process.

B. Variable-fidelity Optimization Algorithm

A generic variable-fidelity optimization algorithm produces a sequence $\mathbf{x}^{(i)}$, $i = 0, 1, \ldots$, of approximate solutions to (1) (here, $\mathbf{x}^{(0)}$ is the initial design) as[16]

$$\mathbf{x}^{(i+1)} = \arg\min_{\mathbf{x}} H(\mathbf{s}^{(i)}(\mathbf{x})), \tag{2}$$

where $\mathbf{s}^{(i)}(\mathbf{x}) = [C_{l.s}{}^{(i)}(\mathbf{x})\ C_{d.s}{}^{(i)}(\mathbf{x})\ A_s{}^{(i)}(\mathbf{x})]^T$ is a surrogate model at iteration i. The surrogate model is a suitably corrected low-fidelity model $\mathbf{c}$. In this work, manifold mapping[20,21,22] is utilized to correct the low-fidelity model during each design iteration.

C. Manifold Mapping

Manifold mapping (MM) is a response correction technique capable of comprehensive exploitation of available high-fidelity model data. The MM surrogate model is defined in its basic version as[20,21,22]

$$\mathbf{s}^{(i)}(\mathbf{x}) = \mathbf{f}(\mathbf{x}^{(i)}) + \mathbf{S}^{(i)}\left(\mathbf{c}(\mathbf{x}) - \mathbf{c}(\mathbf{x}^{(i)})\right) \tag{3}$$

with $\mathbf{S}^{(i)}$ being the 3×3 correction matrix (in general, the size of **S** is equal to the number of the components in **c**, **f**, and **s**) and is defined as

$$\mathbf{S}^{(i)} = \mathbf{\Delta F} \cdot \mathbf{\Delta C}^{\dagger}, \tag{4}$$

where

$$\mathbf{\Delta F} = [\, f(\mathbf{x}^{(i)}) - f(\mathbf{x}^{(i-1)}) \quad \ldots \quad f(\mathbf{x}^{(i)}) - f(\mathbf{x}^{(\max\{i-n,0\})})], \tag{5}$$

$$\mathbf{\Delta C} = [\, c(\mathbf{x}^{(i)}) - c(\mathbf{x}^{(i-1)}) \quad \ldots \quad c(\mathbf{x}^{(i)}) - c(\mathbf{x}^{(\max\{i-n,0\})})]. \tag{6}$$

The pseudoinverse, denoted by †, is defined as[20,21,22]

$$\mathbf{\Delta C}^{\dagger} = \mathbf{V}_{\mathbf{\Delta C}} \mathbf{\Sigma}^{\dagger}_{\mathbf{\Delta C}} \mathbf{U}^{T}_{\mathbf{\Delta C}}, \tag{7}$$

where $\mathbf{U}_{\Delta C}$, $\sum_{\Delta C}$, and $\mathbf{V}_{\Delta C}$ are the factors in the singular value decomposition of the matrix $\mathbf{\Delta C}$. The matrix $\sum_{\Delta C}{}^{\dagger}$ is the result of inverting the nonzero entries in $\sum_{\Delta C}$, leaving the zeroes invariant.

D. Gradient-enhanced Manifold Mapping

If derivatives of both the low- and high-fidelity models are available, the correction matrix $\mathbf{S}^{(i)}$ can be determined directly using respective model Jacobians. More specifically, we have[24]

$$\mathbf{S}^{(i)} = \mathbf{J}_f(\mathbf{x}^{(i)}) \cdot \mathbf{J}_c(\mathbf{x}^{(i)})^{\dagger}, \tag{8}$$

where

$$\mathbf{J}_c(\mathbf{x}^{(i)})^{\dagger} = \mathbf{V}_{\mathbf{J}_c} \mathbf{\Sigma}^{\dagger}_{\mathbf{J}_c} \mathbf{U}^{T}_{\mathbf{J}_c}. \tag{9}$$

Here, $\mathbf{U}_{Jc}$, $\sum_{Jc}$, and $\mathbf{V}_{Jc}$ are the factors in the singular value decomposition of the low-fidelity model Jacobian $\mathbf{J}_c$ at the current design $\mathbf{x}^{(i)}$. In the case of scalar responses, the Jacobians are replaced by their respective gradients. In this work, the Jacobians (and gradients) are calculated cheaply adjoint sensitivity information.[23]

III. Demonstration Case

The proposed approach is demonstrated on a benchmark case for aerodynamic shape optimization involving transonic inviscid flow (see, e.g., Jie *et al.*[22]). This section describes the problem, design variables, computational fluid dynamics modeling, and the optimization results. The proposed gradient-enhanced manifold mapping (GMM) technique is compared with the basic manifold mapping (MM) technique in terms of quality and computational cost.

A. Problem Description

The objective is to minimize the drag coefficient (C_d) of modified NACA 0012 airfoil section in steady inviscid flow at a free-stream Mach number of $M_\infty = 0.85$, and an angle of attack of $\alpha = 0°$, subject to a minimum thickness constraint. The optimization problem is stated as

$$\min_{\mathbf{l} \le \mathbf{x} \le \mathbf{u}} C_d, \tag{10}$$

where **x** is the vector of design variables, and **l** and **u** are the lower and upper bounds, respectively. In our implementation, the objective function is set as $H(\mathbf{f}(\mathbf{x})) = C_d$. The thickness constraint is stated as

$$z(x) \ge z(x)_{baseline}, \tag{11}$$

where $z(x)$ is the airfoil thickness, $x \in [0,1]$ is the chord-wise location, and $z(x)_{baseline}$ is the thickness of the baseline airfoil, which is a modified version of the NACA 0012, defined as

$$z(x)_{baseline} = \pm 0.6\left(0.2969\sqrt{x} - 0.1260x - 0.3516x^2 + 0.2843x^3 - 0.1036x^4\right). \quad (12)$$

The thickness constraint is handled directly.

B. Design Variables

Due to symmetry in the demonstration case, only the upper surface is parameterized. B-spline curves (see, e.g., Farin[25]) are used in this work for the shape parametrization. The B-spline control points are used as design variables as shown in Fig. 1. The leading- and trailing-edge control points are fixed. The other control points are free to move in the vertical direction with their horizontal locations fixed during the optimization. In this work, the number of variables is varied. In particular, the solution to (10) is attempted using 5, 8, 10, and 15 design variables. The initial shape is set by fitting it to the modified NACA 0012 of (12). The lower bound on each x_i is set as 0.0, and the upper bound as 1.0.

C. Variable-fidelity Modeling

The compressible Euler equations are used to simulate the transonic inviscid fluid flow past the airfoils shapes. The Stanford University Unstructured (SU^2) computer code[26] is utilized for the simulations. The governing equations are solved with an implicit density-based formulation, and the convective fluxes are calculated using the second order Jameson-Schmidt-Turkel (JST) scheme[27]. Three multi-grid levels are used for solution acceleration, and asymptotic convergence to a steady state solution is obtained in each case. The flow solver convergence criterion is the one that occurs first of the two: (i) the change in the drag coefficient value over the last 100 iterations is less than 10^{-4}, or (ii) a maximum number of iterations of 1,000 is met. An O-type computational mesh is generated using Pointwise[28] (see Figure 2). Only the half-plane is considered since the airfoil is symmetrical and the angle of attack is fixed at zero. The farfield boundary is set 55 chord lengths away from the airfoil surface, and the mesh density is controlled by the number of cells on the airfoil surface and the number of cells normal to the surface. The results of a grid convergence study, given in Table 1, revealed that a 512 × 512 mesh is required for convergence within 0.2 drag count (1 drag count is $\Delta C_d = 10^{-4}$) when compared with the next mesh. Distance to the first grid point is 0.0015 chord lengths. The flow simulation for Mesh 5 takes about 10.3 min. An adjoint solution for the drag coefficient take approximately the same amount of time. For the optimization studies, Mesh 5 is used as the high-fidelity model **f**, and Mesh 3 as the low-fidelity model **c**. For the low-fidelity model, the maximum number of solver iterations is set to 300.

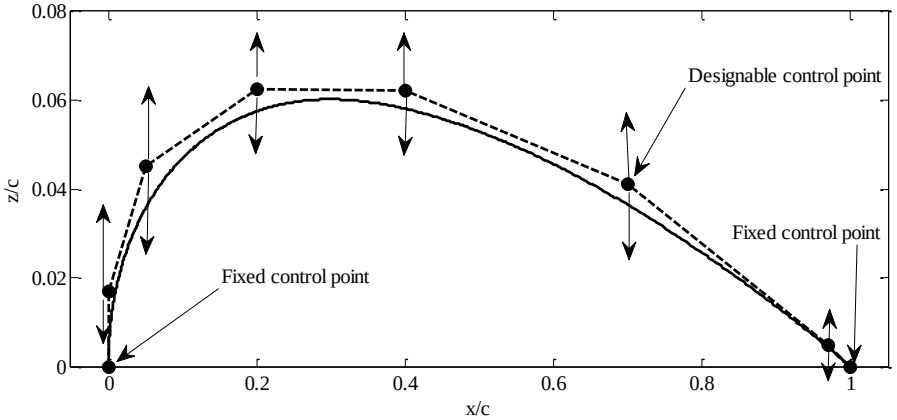

Figure 1. B-spline parameterization for the upper surface of the airfoil.

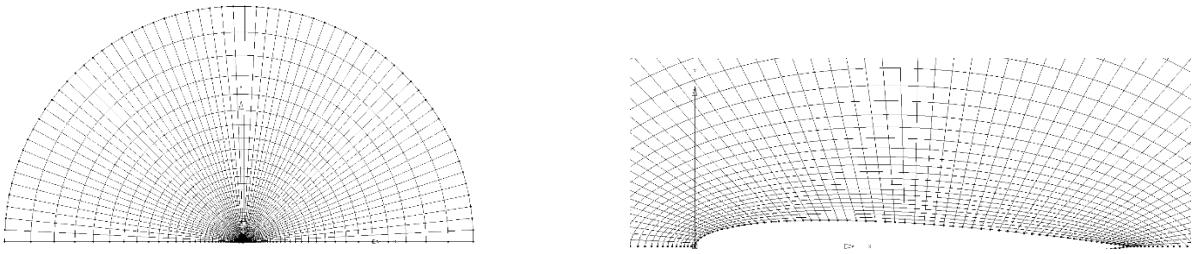

(a) **(b)**

Figure 2. The half-plane O-mesh used in the inviscid model: (a) farfield view, (b) a view close to the surface.

Table 1. Grid convergence study for the baseline shape at $M_\infty = 0.85$ and $\alpha = 0.0°$.

Mesh	Grid Size	C_l (cts)	C_d (cts)	Simulation Time* (min)
1	32 × 32 (961)	0.0	409.4050	0.07
2	64 × 64 (3,969)	0.0	460.5103	0.16
3	128 × 128 (16,129)	0.0	466.6935	0.51
4	256 × 256 (65,025)	0.0	467.9302	1.65
5	512 × 512 (261,121)	0.0	468.1746	10.33
6	1,024 × 1,024 (1,046,529)	0.0	468.3757	71.10

* Computed with 20 processors. Flow solution only.

D. Optimization Results

The optimization results are presented in Table 2. Figure 3 shows the baseline and optimized shapes and their correpsonding pressure coefficient distributions. In all optimiztion runs the thickness constraint is fulfilled. The results show that using the MM technique and 8 design variables the drag coefficient is reduced from 478 d.c. to around 96.5 d.c. (or −79.8%). Using the GMM technique, and the same number of design variables, a comparable design is obtained. That particular design has a drag coefficient value of 94.7 d.c., and a similar shape (as can be seen in Fig. 3). Table 3 shows that the designs are gid indepented down to 0.1 d.c.

In terms of computational cost, the MM technique needed 9 high-fidelity model evaluations and 2,045 low-fidelity ones, which is equivalent to around 89 high-fidelity model evaluations. The GMM technique, on the other hand, needed 5 high-fidelity model evaluations and 159 low-fidelity ones, which is equivalent to around 13 high-fidelity model evaluations. The total time for the MM technique is 1,625 min, whereas the total time for the GMM technique is 475 min. It should be noted here that the GMM technique solves for the primary flow solution as well as the adjoint solution, whereas the MM technique only solves for the primary flow solutions. Nevertheless, in terms of time, the GMM technique needed 70.8% less time than the MM technique.

The quality of the design changes significantly depending on the number design variables. The best overall design obtained by the GMM technique is the one with 10 design variables. That design has a drag coefficient of around 82.2 d.c. (or 82.8% less than the baseline design). In this case, the computational cost is equivalent to 9 high-fidelity model evaluations, or around 273 min.

Table 2. Optimization results of the demonstration case using manifold mapping (MM) with 8 design variables (DVs) and the gradient-enhanced manifold mapping (GMM) using 5, 8, 10, and 15 DVs.

Parameter/Method	Baseline	MM	GMM			
		8DV	5DV	8DV	10DV	15DV
C_l (l.c.)	0.0	0.0	0.0	0.0	0.0	0.0
C_d (d.c.)	478.05	96.49	233.6	94.7	82.2	91.3
N_c	–	2,045	68	159	99	38
N_f	–	9	4	5	3	2
N_{tot}	–	≈ 89	≈ 8	≈ 13	≈ 9	≈ 4
t_c (min)	–	1,461	116.0	285.3	171.3	65.5
t_f (min)	–	165.4	134.5	189.7	101.7	68.94
t_{tot} (min)	–	1,626	250.5	475.0	273.0	134.4

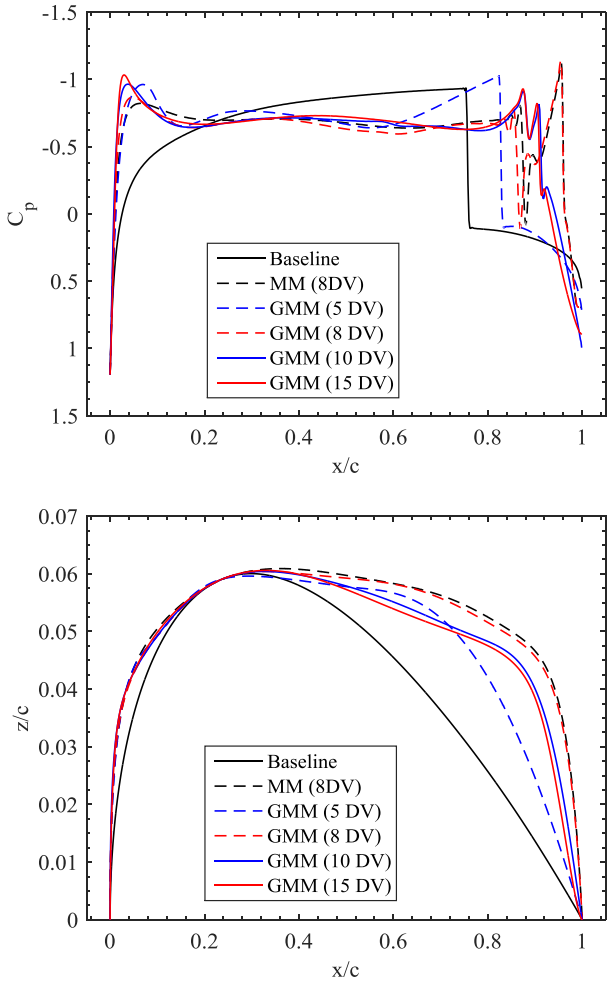

Figure 3. Optimization results of the demonstration case showing the baseline and optimized shapes (bottom) and their corresponding pressure coefficient distributions (top).

Table 3. Grid convergence study for the GMM optimized shape with 10 DVs at $M_\infty = 0.85$ and $\alpha = 0.0°$.

Mesh	Grid Size	C_l (cts)	C_d (cts)	Simulation Time* (min)
1	32 × 32 (961)	0.0	224.6944	0.07
2	64 × 64 (3,969)	0.0	104.2459	0.17
3	128 × 128 (16,129)	0.0	82.0873	0.53
4	256 × 256 (65,025)	0.0	82.4705	1.85
5	512 × 512 (261,121)	0.0	82.1600	11.43
6	1,024 × 1,024 (1,046,529)	0.0	82.2064	84.30

* Computed with 20 processors. Flow solution only.

IV. Conclusion

A computationally efficient optimization methodology for aerodynamic design using variable-fidelity models and gradient-enhanced manifold mapping is presented. Inexpensive gradient information is used to improve the surrogate model creation as well as accelerating the optimization process. The proposed approach is applied to constrained airfoil drag minimization in two-dimensional inviscid transonic flow. The results show that satisfactory optimized designs can be obtained at a low computational cost.

References

[1]Leoviriyakit, K., Kim, S., and Jameson, A., "Viscous Aerodynamic Shape Optimization of Wings including Planform Variables," *21st Applied Aerodynamics Conference*, Orlando, Florida, June 23-26, 2003.

[2]Braembussche, R.A., "Numerical Optimization for Advanced Turbomachinery Design," In *Optimization and Computational Fluid Dynamics*, Thevenin, D. and Janiga, G., editors, Springer, 2008, pp. 147-189.

[3]Mader, C. A., and Martins J. R. R. A, "Derivatives for Time-Spectral Computational Fluid Dynamics Using an Automatic Differentiation Adjoint," *AIAA Journal*, Vol. 50, No. 12 (2012), pp. 2809-2819. doi: 10.2514/1.J051658

[4]Mousavi, A., and Nadarajah, S., "Heat Transfer Optimization of Gas Turbine Blades Using an Adjoint Approach," *13th AIAA/ISSMO Multidisciplinary Analysis Optimization Conference*, AIAA Paper 2010-9048, Fort Worth, Texas, Sept. 13-15, 2010.

[5]Leung, T.M., and Zingg, D.W., "Aerodynamic Shape Optimization of Wings Using a Parallel Newton-Krylov Approach," *AIAA Journal*, Vol. 50, No. 3 (2012), pp. 540-550.

[6]Epstein, B., and Peigin, S., "Constrained Aerodynamic Optimization of Three-Dimensional Wings Driven by Navier-Stokes Computations", *AIAA Journal*, Vol. 43, No. 9 (2005), pp. 1946-1957.

[7]Nocedal, J., and Wright, S.J., *Numerical Optimization*, Springer, 2006.

[8]Kim, S., Hosseini, K., Leoviriyakit, K., and Jameson, A., "Enhancement of Class of Adjoint Design Methods via Optimization of Parameters", *AIAA Journal*, Vol. 48, No. 6 (2010), pp. 1072-1076.

[9]Schmidt, S., Gauger, N., Ilic, C., Schulz, V., "Three Dimensional Large Scale Aerodynamic Shape Optimization based on Shape Calculus", *41st AIAA Fluid Dynamics Conference and Exhibit*, AIAA Paper 2011-3718, Honolulu, Hawaii, June 27-30, 2011.

[10]Queipo, N.V., Haftka, R.T., Shyy, W., Goel, T., Vaidyanathan, R., and Tucker, P.K., "Surrogate-Based Analysis and Optimization," *Progress in Aerospace Sciences*, Vol. 41, No. 1, 2005, pp. 1-28

[11]Forrester, A.I.J., and Keane, A.J., "Recent advances in surrogate-based optimization," *Progress in Aerospace Sciences*, Vol. 45, No. 1-3, 2009, pp. 50-79.

[12]Koziel, S., Echeverría-Ciaurri, D., and Leifsson, L., "Surrogate-based methods," in S. Koziel and X.S. Yang (Eds.) *Computational Optimization, Methods and Algorithms*, Series: Studies in Computational Intelligence, Springer-Verlag, pp. 33-60, 2011.

[13]Alexandrov, N.M., Lewis, R.M., Gumbert, C.R., Green, L.L., and Newman, P.A., "Optimization with Variable-Fidelity Models Applied to Wing Design," *38th Aerospace Sciences Meeting & Exhibit*, Reno, NV, AIAA Paper 2000-0841, Jan. 2000.

[14]Robinson, T.D., Eldred, M.S., Willcox, K.E., and Haimes, R., "Surrogate-Based Optimization Using Multifidelity Models with Variable Parameterization and Corrected Space Mapping," *AIAA Journal*, vol. 46, no. 11, 2008.

[15]Koziel, S., Cheng, Q.S., and Bandler, J.W., "Space mapping," *IEEE Microwave Magazine*, vol. 9, no. 6, pp. 105-122, Dec. 2008.

[16]Koziel, S. and Leifsson, L., "Knowledge-based airfoil shape optimization using space mapping," *30th AIAA Applied Aerodynamics Conference*, New Orleans, Louisiana, June 25-28, 2012.

[17]Koziel, S., and Leifsson, L., "Adaptive Response Correction for Surrogate-Based Airfoil Shape Optimization," *30th AIAA Applied Aerodynamics Conference*, New Orleans, Louisiana, June 25-28, 2012.

[18]Koziel, S., and Leifsson, L., "Multi-Fidelity Airfoil Optimization with Adaptive Response Prediction," *14th AIAA/ISSMO Multidisciplinary Analysis and Optimization Conference*, Sept. 17-19, Indianapolis, Indiana, 2012.

[19]Koziel, S., and Leifsson, L., "Surrogate-Based Aerodynamic Shape Optimization by Variable-Resolution Models," *AIAA Journal*, vol. 51, no. 1, 2013, pp. 94-106.

[20]Echeverría-Ciaurri, D., and Hemker, P.W., "Manifold Mapping: a Two-Level Optimization Technique," *Computing and Visualization in Science*, 11, pp. 193-206, 2008.

[21]Koziel, S., and Echeverría-Ciaurri, D., "Reliable Simulation-Driven Design Optimization of Microwave Structures Using Manifold Mapping," *Progress in Electromagnetic Research B* (PIER B), 26, pp. 361-382, 2010.

[22]Jie, R., Leifsson, L., Koziel, S., and Tesfahunegn, Y., "Multi-fidelity Aerodynamic Shape Optimization Using Manifold Mapping," *AIAA Science and Technology Forum and Exposition (SciTech2016)*, San Diego, CA, 2016.

[23]Jameson, A., "Aerodynamic Design via Control Theory," *Journal of Scientific Computing*, Vol. 3, 1988, pp. 233-260.

[24]Koziel, S., Ogurtsov, S., Bandler, J.W., and Cheng, Q.S., "Reliable space mapping optimization integrated with EM-based adjoint sensitivities," *IEEE Trans. Microwave Theory Tech.*, 61, pp. 3493-3502, 2013.

[25]Farin G., *Curves and Surfaces for Computer Aided Geometric Design*, Boston, MA: Academic Press, 1993.

[26]Palacios, F., Colonno, M. R., Aranake, A. C., Campos, A., Copeland, S. R., Economon, T. D., Lonkar, A. K., Lukaczyk, T. W., Taylor, T. W. R., and Alonso, J. J., "Stanford University Unstructured (SU^2): An open-source integrated computational environment for multi-physics simulation and design," AIAA Paper 2013-0287, 51st *AIAA Aerospace Sciences Meeting and Exhibit*, Grapevine, Texas, USA, 2013.

[27]Jameson, A., Schmidt, W., and Turkel, E., "Numerical Solution of the Euler Equations by Finite Volume Methods Using Runge-Kutta Time-Stepping Schemes," AIAA 1981-1259, *AIAA 14th Fluid and Plasma Dynamic Conference*, Palo Alto, CA, June 23-25, 1981.

[28]Pointwise V17.3R2, Pointwise Inc., 213 South Jennings Avenue, Fort Worth, Texas, 76104-1107, USA.